Target-Independent Quantitative Thermography

Turbomachinery and Heat Transfer Laboratory
Iliya Romm , Asst. Prof. Beni Cukurel
Technion – Israel Institute of Technology

MOTIVATION

Infrared (IR) imaging is a nondestructive, noncontact evaluation technique used in diagnostics and monitoring, which is able to resolve surface details and radiation gradients. However, converting image intensity values into temperatures usually requires precise knowledge about the target (specifically, its spectral emissivity), or an ad-hoc calibration. The present research attempts to shift this paradigm.

THEORY & MODEL

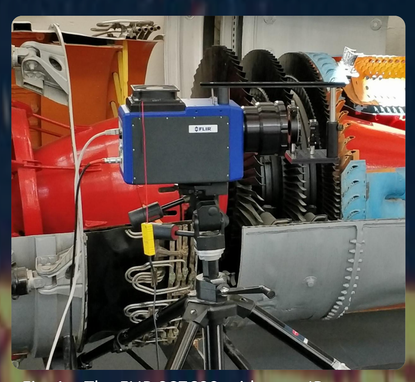

Fig. 1 – The FLIR SC7600 mid-wave IR camera.

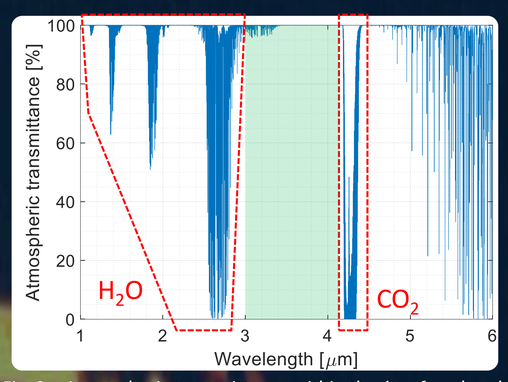

Fig. 2 – Atmospheric transmittance within the $1-6\mu m$ band.

The infrared camera used in this study (Fig.1) is sensitive to the $1-6\mu m$ wavelength band of the EM spectrum. The radiance received by the camera consists of several contributors:

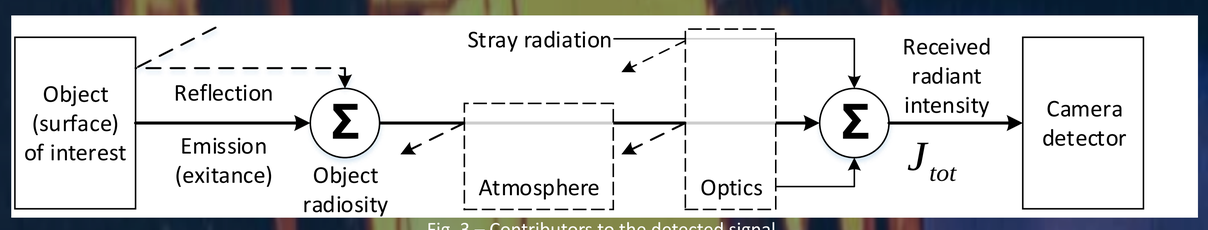

Fig. 3 – Contributors to the detected signal.

The response of a single camera pixel can be expressed by eq. (1):

$$\underbrace{J_{tot}\left(T;\Delta\lambda\right)}_{\substack{\text{Detected radiation}\\ \text{through a filter}\\ \text{allowing }\Delta\lambda}} = \int_{\Delta\lambda} \underbrace{\mathcal{R}(\lambda)}_{\substack{\text{Detector}\\ \text{spectral}\\ \text{response}}} \cdot \underbrace{\tau_{atm}(\lambda)}_{\substack{\text{Atmospheric}\\ \text{tramsmittance}}} \cdot \underbrace{\tau_{optics}(\lambda)}_{\substack{\text{Lens and filter}\\ \text{transmittance}}} \cdot \underbrace{\varepsilon(\lambda,T)}_{\substack{\text{Target}\\ \text{spectral}\\ \text{emissivity}}} \cdot \underbrace{2hc^2\lambda^{-5}\cdot\left[\exp\left(\frac{hc}{k_B\lambda T}\right)-1\right]^{-1}}_{\text{Blackbody Planck radiation}} d\lambda \quad (1)$$

Where the final goal is to obtain $\boldsymbol{T}$.

IMAGE FUSION

A "photoquantity" is a consistent scale resulting from integrating incoming light over the spectral response of a particular camera system.

The camera measurement equation is expressed by:

$$DL = R \cdot IT^{P(R)} + BF + v(t) \quad (2)$$

where DL is the digital level, IT is integration time, R is the photoquantity, P is a nonlinearity coefficient, BF is a bias frame (i.e. time invariant noise) and $v(t)$ is temporal noise.

$v(t)$ is assumed to be zero-mean and thus can be negated when a sufficient amount of images is averaged. BF can be estimated from series of low ITs [1]. Finally, to obtain R and P, $N \geq 2$ distinct ITs are chosen, the corresponding DLs are recorded, and a log-linear optimization problem is solved:

$$\begin{bmatrix}\log(DL_1)\\ \vdots \\ \log(DL_N)\end{bmatrix} = \begin{bmatrix}1 & \log(IT_1)\\ \vdots & \vdots \\ 1 & \log(IT_N)\end{bmatrix}\begin{bmatrix}\log(R)\\ P\end{bmatrix} \quad (3)$$

The acquisition at several ITs extends the dynamic range of the detector, allowing it to capture both brighter and dimmer regions of a scene that could otherwise not be captured in a single-IT photo, Fig.5.

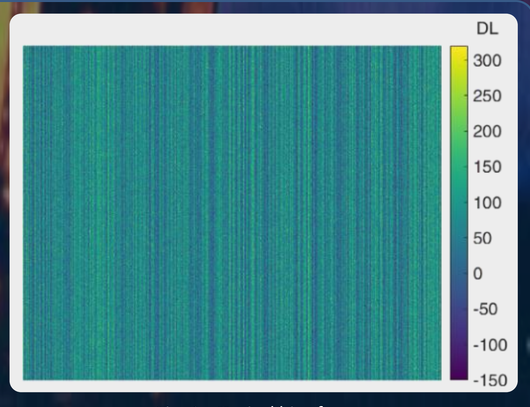

Fig. 4 – Typical bias frame.

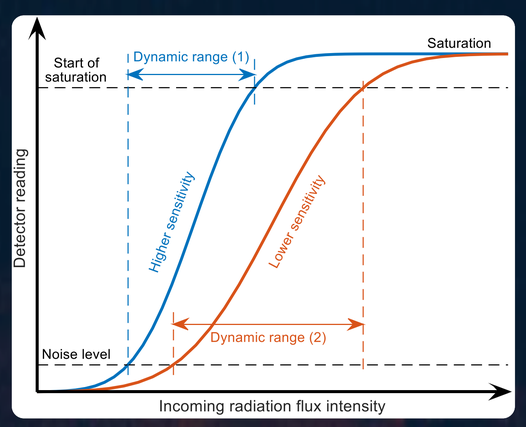

Fig. 5 – Manipulation of a detector's dynamic range via the choice of IT [2].

The most valuable outcome of image fusion in a quantitative context is increased tonal fidelity (bit resolution), compared to the 14-bit camera output.

Fig.6 depicts this procedure being done for two sets of frames: the scene frames and frames where the target is obscured by some physical barrier (called "dark frames"). Subtracting the dark frame from the scene frame eliminates the unwanted signal contributions from of the optics and the stray radiation.

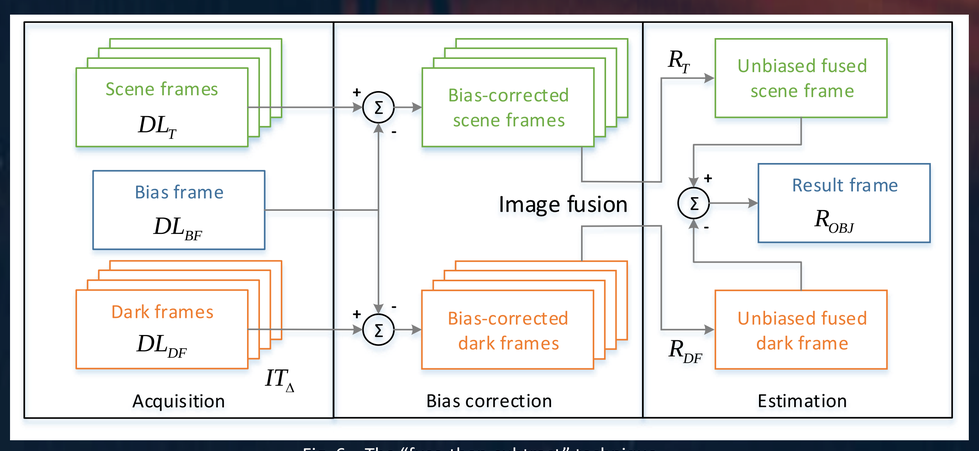

Fig. 6 – The "fuse-then-subtract" technique.

MULTISPECTRAL IMAGING

Multispectral imaging is the introduction of several alternate band-pass optical filters into the optical path to limit the spectral composition of the detected radiation. The reasons to use this technique are:

- Radiometry of non-black bodies is inherently underdetermined since different combinations of emissivity and temperature can yield the same signal, and both are unknown.
  → Each spectrally-distinct measurements serves as an additional data point.
- The exact atmospheric composition (e.g. Fig.2) in the optical path (mainly humidity and CO_2 concentration) cannot be measured reliably in many cases, let alone controlled.
  → Carefully choosing filters in bands where the atmosphere is transparent can negate its effect.

After choosing filters, calibration is performed using a black body radiator, once per optical configuration, resulting in an approximation of eq. (1) having the form [3]:

$$J_{tot}(T;\Delta\lambda) \propto R_{BB} \approx \frac{a_0}{\exp\left[\frac{a_1}{T}+\frac{a_2}{T^2}\right]-1} \quad (4)$$

Where each configuration is fully characterized by the fitted coefficients a_i ($r^2 > 0.999$).

Following a multispectral measurement, $R_1 \ldots R_N$ values corresponding to the N filters are used to fit an equation where (4) is multiplied by a preselected emissivity model $\varepsilon(\lambda)$ of $[1, N-1]$ parameters.

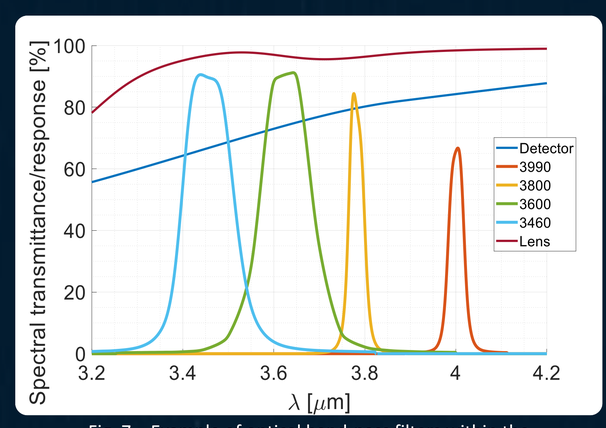

Fig. 7 – Example of optical band-pass filters within the 3-4.1μm atmospheric window (shown in green in Fig. 2).

This results in a set of possible $\{\varepsilon, T\}$ combinations which must be disambiguated further.

PRELIMINARY RESULTS

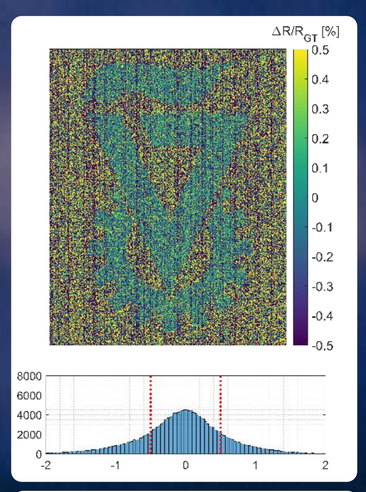

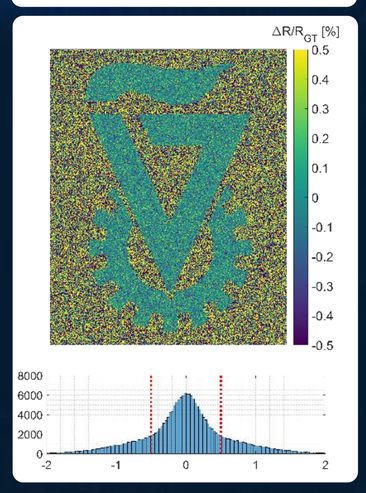

Fig. 9 – Comparison of relative errors after image fusion with NUC (top) and FTS (bottom).

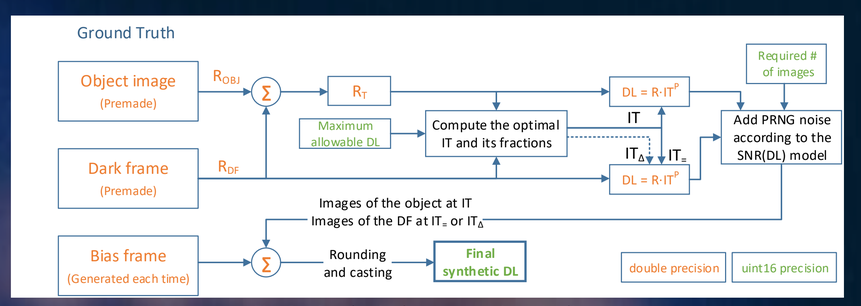

Fig. 8 – Synthetic data generation pipeline.

- An algorithm was developed to estimate the bias frame (Fig. 4) from measured dark frames.
- A synthetic data analysis comparing the proposed technique to the traditional NUC-based alternative demonstrated the superiority of the new technique.
- The analysis also showed how the estimation error is affected by averaging more images vs using more ITs.

Images averaged	200°C			400°C			600°C		
512	3.051	2.314	2.008	13.06	10.48	10.51	39.76	32.17	28.61
256	4.339	3.343	2.834	18.47	16.32	13.09	60.36	45.47	40.36
128	6.183	4.717	4.015	26.08	23.15	21.03	85.26	72.19	57.13
64	8.734	6.686	5.665	39.27	32.67	29.77	111.8	102.2	93.63
32	12.36	9.436	8.02	55.39	41.66	42.06	170.1	144.6	132.5
16	17.48	13.41	11.34	78.7	65.24	59.51	240.8	204.5	187
8	24.76	18.92	16.03	110.9	92.62	83.78	342.4	289.6	264
4	34.96	26.73	22.67	156.5	130.4	119.2	484.2	409.5	374.9
2	49.54	37.88	32.1	221.8	185	168	681.6	578.2	529.2
1	70.09	53.53	45.53	313.7	261.7	237.9	969.7	817.7	750.8
	4	8	12	4	8	12	4	8	12
	Number of ITs			Number of ITs			Number of ITs		

Fig. 10 – L^2 norms between ground-truth and R values estimated using FTS. Based on synthetic data.

- Synthetic analysis findings were experimentally validated, where FTS achieved a reduction of two or more orders of magnitude in the relative error $(|\Delta R|/R_{GT})$ compared to other methods.
- The response characterization method allows acquisitions at a broader range of integration times, since it does not require the accommodation of reference measurements at the margins of the dynamic range.

CONCLUSIONS

- The proposed technique appears to eliminate the need for a NUC procedure and on-site calibration.
- HDR-like IR image blending is able to produce wide dynamic-range, high-fidelity images.

FUTURE WORK

- Incorporation of spatial information into the $\varepsilon - T$ optimization to eliminate some local minima.
- Adaptation of the technique to unsteady phenomena such as combustion or metallurgy processes.
- Automatic selection and/or blending of emissivity models.

REFERENCES

[1] I. Romm, M. Lev, B. Cukurel (2015) Empirical compensation of reciprocity failure and integration time nonlinearity in a mid-wave infrared camera, Measurement Science and Technology, 27 025005. http://dx.doi.org/10.1088/0957-0233/27/2/025005.
[2] I. Romm, B. Cukurel (2018) Quantitative image fusion in infrared radiometry, Measurement Science and Technology. https://doi.org/10.1088/1361-6501/aaab3c.
[3] P. Saunders, D.R. White (2003) Physical basis of interpolation equations for radiation thermometry, Metrologia, 40 195. https://doi.org/10.1088/0026-1394/40/4/309